A weather forecast-based control for the improvement of PCM enhanced radiant floors

Silvia Cesari [*], Giuseppe Emmi, Michele Bottarelli

Department of Architecture, University of Ferrara, Via Quartieri 8, Ferrara 44121, Italy

A B S T R A C T

Significant energy savings and thermal comfort improvement related to radiant floor systems may not be achieved when underfloor heating/cooling is adopted in lightweight building envelopes. Phase change materials (PCMs) are suitable candidates for providing the necessary thermal inertia with a minimum effect on the construction technology. Impacting variables like internal heat gains, weather conditions and dynamic energy price require the adoption of advanced control strategies to ensure and maximise the energy benefits of PCMs. Despite the potential of model predictive control using weather prediction data has been widely examined by the literature, there is a lack of studies experimentally analysing their implementation in PCM enhanced radiant floor systems. Within the H2020 European project IDEAS the integration of PCMs in a radiant floor system was examined by the University of Ferrara through numerical and experimental investigation. A first prototype was then installed in a small experimental building characterised by a low thermal capacity. Analysis of the monitoring data for the heating period showed that solar radiation strongly impacts on the lightweight building envelope in a short time. Without suitable control, the contribution of PCM that slowly reduced its heat flux during its transition, together with solar heat gains, resulted in an excessive increase in indoor air temperature, wasting the PCM energy saving potential. The aim of the study is the evaluation of a control strategy to improve the management of PCM enhanced radiant floor systems in relation to forthcoming weather conditions in lightweight buildings. The control routine was implemented in the corresponding dynamic energy model in TRNSYS. Results estimated achievable energy saving equal to about 4% and 8% on the heating and the cooling energy demand respectively.

1. Introduction

The tendency to implement lightweight building elements has been steadily increasing in the last years. Current construction trends demand speed and ease of assembly and lightweight buildings enable the use of prefabrication and on-site assembly, which is cost-effective and less time-consuming [1,2]. However, the dynamic behaviour of thermal mass and its positive contribution to delay heat fluxes and regulate indoor temperature fluctuations has been recognised [3,4] in contrast to the rigid thermal performance of lightweight building envelopes, which raises the need for heating and cooling systems. Phase change materials (PCMs) are considered as an interesting alternative to sensible storage in heavyweight constructions, with a theoretical volumetric storage density of up to 15 times higher than traditional storage materials [5]. PCMs can be used to shift the cooling or heating load from the peak period to the off-peak period [6,7]. For this reason, they are often integrated in

radiant floor (RF) systems.

RF is a low-temperature heating system which provides uniform temperature distribution, does not produce noise, cause drafts, and ensures the efficient use of space [8,9]. Nevertheless, enhanced energy performance and improved indoor thermal comfort may not be achieved when RF is adopted in lightweight buildings, due to the low thermal capacity of the envelope and to the relative long response time of the RF if compared to other terminal units like fan coils.

RF systems integrated with PCMs provide efficient energy storage and release in the heating period as well as effective buffering of internal gains in the cooling season [10]. In winter the constant temperature heat storage of the PCM layer is able to accumulate any renewable heating loads as they become available during the daytime (solar radiation, etc.), and to release them at comfort temperature during the night. In summer the embedded PCM layer can provide enough thermal inertia at comfort temperature to absorb thermal loads, which can then be discharged by any intermittent renewable cooling source as soon as they

---

Nomenclature

Acronyms

ACS	Advanced control strategies
EPS	Expanded polystyrene
FEP	Fluorinated ethylene propylene
FCS	Floor control strategy
HDPE	High-density polyethylene
HP	Heat pump
IDEAS	Novel building integration designs for increased efficiencies in advanced climatically tunable renewable energy systems
ITES	Intra-day/season thermal energy storage
MES	Multi-source/sink energy sub-system
MPC	Model predictive control
PCM	Phase change material
PE	Polyethylene
PID	Proportional, integral and derivative
RCS	Reference case study
RES	Renewable energy systems
RF	Radiant floor
TCS	Traditional control strategies
WP3	Work package n.3

Symbols

c	heat capacity [kJ/(kg·°C)]
$\dot{m}$	mass flow rate [kg/h]
Q	heat transfer [kJ]
T	temperature [°C]
Δt_{step}	simulation timestep [h]

Subscripts

C	cooling period
conc	concrete
ext	outdoor air
H	heating period
in	inlet
out	outlet
RF	radiant floor
set	setpoint
ti	ThinICE

---

become available (ventilation, geothermal, etc.). A growing body of literature has been demonstrating the ability of RF systems to achieve heating energy savings when incorporating a PCM layer [11–17]. At the same time, a large number of studies have also been investigating the cooling potential of PCMs embedded into RF systems [18]. A RF integrated with double PCM layers having two different melting temperatures – one at 38 °C for space heating and another at 18 °C for space cooling – was numerically analysed by Jin and Zhang [19]. A two-layer PCM RF structure with heat storage layer below and cold storage layer above was numerically investigated by Xu et al. [20]. Again, Sun et al. carried out the experimental investigation of a RF system containing two types of inorganic PCMs [21].

Several studies showed that the application of a RF integrated with PCM can significantly lower the building heating demand by up to 45% [22]. The reduction of peak loads and of the overall energy demand for space air-conditioning, along with the extended lifetime of auxiliary system due to efficient operation, all bring to reduced operation costs [23–25]. Indeed, RF systems that are subject to controlled charging and discharging are charged preferably during off-peak electricity pricing hours, providing benefits due to demand shifting [10,19]. Therefore, the integration of PCMs in active systems has the potential to shift peak load, reduce energy cost, enhance the thermal efficiency of buildings, and eventually reduce air pollution and mitigate global warming [26,27]. However, the adoption of PCMs requires high initial capital costs. For this reason, the application of a suitable control strategy has become essential to maximise the energy benefits of PCMs and optimise their use in buildings to lower investment costs [28]. Nevertheless, research on this subject area is still limited.

A large number of different control strategies have been developed during the last decades and are being increasingly improved. Control methods can be divided into two main categories: traditional control strategies (TCS) and advanced control strategies (ACS) [29]. The former include two different approaches: sequencing control, which uses on/off control as the main logic, and process control, based on proportional, integral and derivative (PID) control [30]. These methods operate on the base of the signal received by basic sensors such as thermostats, pressure switches or humidistats. TCS, that are the simplest control method, are significantly limited by the lack of interaction with the external environment, which prevents implementing a highly effective control strategy. Indeed, studies available in literature have uncovered critical issues in the control of radiant systems due to their large thermal inertia

that is difficult to handle with TCS in order to respond to changes in weather or room temperature [31]. Therefore, in light of impacting variables like internal heat gains (occupants, lighting, appliances, solar radiation, etc.), weather conditions and dynamic energy price, the application of TCS results to be extremely modest, thus suggesting the implementation of ACS that allow to consider all the external factors mentioned before [32]. ACS comprise three different types of sub-categories: soft-computing, hard-computing and hybrid control strategies [30,33]. Soft-computing include reinforcement learning, deep learning based on artificial neural network, fuzzy logic controls and agent-based controls. They can deal with imprecision, uncertainty and noisy input producing approximate responses. For these reasons, they are able to give solutions to more sophisticated problems. Among hard-computing control strategies there is auto-tuning PID control, gain-scheduling control, self-tuning control, supervisory/optimal control, model predictive control (MPC) and robust control. The common element among all types of hard-computing strategies is the use of a mathematical/analytical model. Such methods usually require real and precise input data to provide an accurate response in the short time [34]. Finally, hybrid control strategies are a combination of soft and hard control approaches.

With the aim of maximising the pre-cooling potential of RF systems during the cooling season and reducing overheating in the heating period various factors should be simultaneously considered and managed, such as internal heat gains, weather patterns and time varying utility prices [31]. Against this background, MPC approach uses dynamic estimates and predictions of outdoor weather conditions, zone loads and temperatures, and HVAC system models to minimise energy consumption and costs while meeting equipment and thermal comfort requirements. MPC includes data-driven building models estimated and validated using data from an actual building [35–38]. More in detail, among the different functions of MPC, their weather predictive/responsive one is the building capability to predict/respond to climate conditions and implement passive and active measures accordingly. In an experimental study Barzin et al. [39] demonstrated that the use of weather prediction data allowed to achieve energy savings of about 30% and cut costs by nearly 41%. Kelman et al. [40] implemented a MPC strategy based on weather forecast aimed at reducing energy consumption while meeting indoor thermal comfort. Moreover, the advancements of Internet of Things (IoT) and cloud-based solutions made it easier to get information from weather data [41].

Despite a large and growing body of literature has been focusing on the different control strategies aimed to reduce energy consumption [42], ensure peak load shifting and shaving [43], as well as indoor thermal comfort [44,45], the review reported above uncovers a lack of studies investigating the application of control methods to PCM enhanced buildings. Thus, the implementation of suitable control approaches to PCM integrated building components results to be still largely unexplored [46].

Gholamibozanjani and Farid carried out a comprehensive review on the different control strategies applied to PCM enhanced buildings [47]. The analysis mainly focused on ON/OFF approach – also known as hysteresis control – as one of the most adopted in PCM integrated buildings. Indeed, this type of method, included among TCS, is the simplest control approach that changes the objective variables between two states of ON or OFF. One of the main objectives of ON/OFF control is peak load shifting/offsetting, which can not only reduce the peak demand, but it allows to achieve considerable cost savings too. Indeed, it can also implement "price-based" control strategies, which consist in postponing the use of electricity during high wholesale market price periods and using it during cheaper hours. These primary goals bring other important benefits too, like a reduction in the generation of electricity from non-renewable energy sources during periods of peak demand and resilience during times of power outages. In addition, power generation companies usually design their systems based on average load. Therefore, any peak demand requires auxiliary equipment which causes extra cost, maintenance, and pollution.

The application of PCM in RF heating systems where the PCM is charged by using electrical energy during low-demand hours to be used during high-demand hours allows to shift the heating load to off-peak hours, thus reducing electricity costs. Devaux and Farid [48] experimentally investigated the application of a PCM with a melting point ranging between 27 and 29 °C in an underfloor heating system, combined with another PCM having a lower melting point (21.7 °C) integrated in the walls and ceiling of a small hut. It was found that the lower melting point PCM helped to maintain comfort condition, while the PCM integrated in the underfloor heating system created peak load shifting with energy and cost savings of 32% and 42%, respectively. Lin et al. [49] conducted a numerical and experimental study on a paraffin-based PCM integrated in underfloor heating. Electric heater was controlled by either time or temperature. It was ON from 23 p.m. to 7 a.m. if temperature was lower than 65 °C. The total heating energy demand was shifted to off-peak hours. Again, a TCS was applied to a RF enhanced with a PCM having a melting point of 27 °C. A controller was used to maintain indoor temperature at 21 °C. Results evaluated a peak load shifting of 1.1 h/day, with a reduction in electricity cost of 18% [23]. Similarly, a PCM integrated into a RF heating system and regulated by a controller used to switch on a heater when room temperature fell below comfort temperature was experimentally investigated in [50]. Results demonstrated that electricity consumption was shifted by 57%. The necessity to maintain indoor comfort level was adopted as control method also in the application of two different PCMs in a RF [51]. An energy cost saving ranging from 45% to 64% was achieved due to peak load shifting, when comfort level was ensured for 13 h. In 2015 Barzin et al. [12] analysed the implementation of a price-based control strategy in a PCM enhanced underfloor heating in an office building. The heater was switched ON or OFF based on the online dynamic electricity price, price constraint, and desired room temperature. Results estimated an average energy saving of about 18.8% with a corresponding 28.7% of cost saving, while the highest energy and cost savings were equal to 35% and 44.4%, respectively. Differently, there are not many studies on the application of MPC in PCM enhanced buildings. These studies have considered different objective functions such as energy [21], energy cost [52], and PCM performance [53].

Analysis of the literature reviewed above has highlighted that the integration of PCMs in RF systems allows to shift peak load, reduce energy consumption, cut energy-related costs and emissions. However, due to the long response time of the RF, the application of MPC strategies able to simultaneously consider and manage the multiple factors impacting on thermal performance and cost efficiency – such as internal heat gains, weather conditions and dynamic energy price – is essential to ensure and maximise the energy benefits of PCMs. Although the different control methods have been exhaustively analysed by the literature, there is little research investigating their application to PCM enhanced RF systems. Again, despite the potential of MPC using weather prediction data has been widely examined, there is a lack of studies experimentally analysing their implementation in PCM integrated RF systems. The very limited number of works that explored the topic were focused on the simplest control method, the ON-OFF approach.

Against this background, experimental and numerical investigation of a hydronic RF heating system integrated with PCM was carried out by the University of Ferrara [11], Italy, within the H2020 European project IDEAS – Novel building Integration Designs for increased Efficiencies in Advanced Climatically Tunable Renewable Energy Systems – [54]. A first prototype was then installed in an existing experimental building having a low thermal capacity and it has been monitored since August 2020. Analysis of the monitoring data for the heating period showed that overheating conditions occurred during sunny and relative warm days without a suitable control. The development and validation of a suitable control strategy based on weather forecasting data and adaptive setpoint temperatures is here reported.

2. Small-scale prototype

The objective of IDEAS project is the development of a novel low-cost building integrated renewable energy systems (RES) which will cost-effectively exceed current RES efficiencies, generating electricity, heat and cooling, and that will be optimised in different climatic conditions. Within this frame, the work package n.3 (WP3 leader: UNIFE – University of Ferrara, Italy), was focused on the design and integration of a heat pump (HP) technology for space heating and cooling via an intra-day/season thermal energy storage (ITES) and a multi-source/sink energy sub-system (MES). MES was designed according to the functionality of an invertible HP able to exploit different thermal sources/sinks: sun, air (outdoor and waste heat), and ground. ITES represents the thermal buffer to equilibrate different and non-synchronous thermal energy requirements. At seasonal and building footprint, the ITES functionality can be supplied by means of horizontal ground heat exchangers coupled with PCMs. At building and daily scale, the function can be provided by an underfloor heating/cooling system and by a novel PV/T solution, all enhanced with suitable PCMs.

A small-scale prototype of the plant was then installed in TekneHub laboratory of UNIFE. The prototype includes a water-to-water HP (5 kW) which operates by means of two primary loops between two tanks (100 L each one), the former on the source-side and the latter on the user-side. The system can exploit three different thermal sources (ground, sun and air) to optimise the temperature on the source-side for air-conditioning of the spaces. The demo building consists of a central main room and two guard rooms, one adjacent on the east side and one adjacent on the west side to the main room (Fig. 1), having a conditioned volume of 26.00 m^3 and 6.24 m^3 (per guard room) respectively. Values for surface, thickness, and thermal transmittance of the components of the building envelope are reported in Table 1. All the zones had been already equipped with a fan coil, while the PCM integrated RF was installed in the main room in August 2020.

Hydrated salts as PCM encapsulated in high-density polyethylene (HDPE) containers named ThinICE [55] – provided by PCM Products Ltd [56], partner of IDEAS project – were used. Two PCMs with different melting temperatures were chosen: 21 °C for the cooling period and 27 °C for the heating one [57]. The different containers were positioned to obtain three zones (which were separated by an insulation layer in order not to influence each other). The first zone on the north was made of 12 ThinICE filled with S27 and was addressed to evaluate the
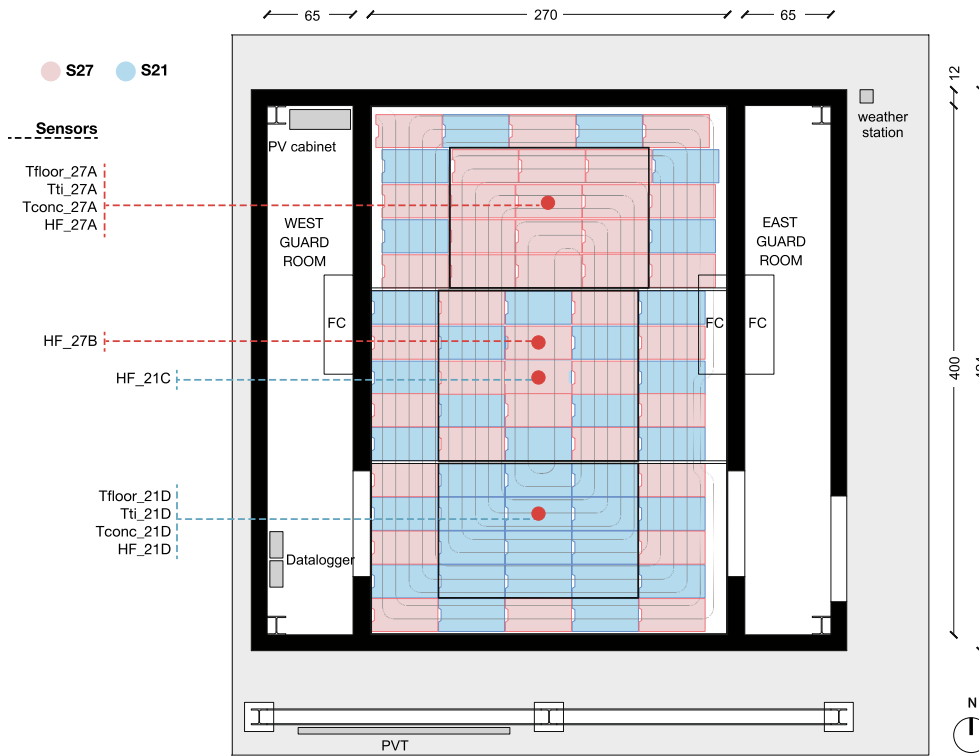
Fig. 1. Plan of the small-scale prototype building with distribution of PCM containers and sensors.

Table 1
Test building physics.

Component	Surface [m²]	Thickness [m]	Thermal transmittance [W/(m²·K)]
Wall	39.84	0.12	0.28
Floor	19.08	0.32	0.28
Roof	19.08	0.06	2.08

behaviour of a full winter solution (red area in Fig. 1). The second area on the south included 12 ThinICE filled with S21 and represented a full summer solution (blue area in Fig. 1). The last zone in the middle was composed of S27 ThinICE alternated to S21 ones, for a total of 15 PCM containers. Macro-encapsulated PCM was installed above a mortar layer including cross-linked PE pipes with a pitch of 100 mm, external diameter of 16 mm and wall thickness 2 mm, positioned above EPS insulation. PCM containers were then embedded in wet sand, so that the floor could be fully inspected (Figs. 2 and 3). Thermal properties of each layer composing the RF, included the selected PCMs, are reported in Table 2.

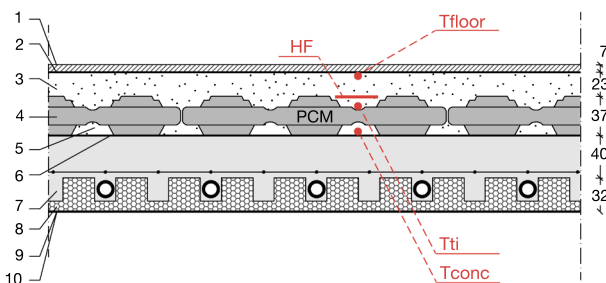**Fig. 3.** RF installation with the positioning of the heat flux meter.

Table 2
Floor structure materials and their thermophysical properties.

Material	Density [kg/m³]	Specific heat [kJ/(kg·K)]	Thermal conductivity [W/(m·K)]
1. Laminate finishing	800	2.00	0.170
2. Nylon sheet (PE)	923	–	–
3. Wet sand	1900	1.90	2.200
4. PCM S27 | S21* [57]	1530	2.20	0.540
5. Wet sand	1900	1.90	2.200
6. Nylon sheet (PE)	923	–	–
7. Mortar	2000	1.00	1.700
8. EPS insulation	20	1.45	0.034
9. Nylon sheet (PE)	923	–	–
10. Underfloor mat	9	1.50	0.044

* S27$_{LATENT HEAT}$ = 185 kJ/kg.
 S21$_{LATENT HEAT}$ = 220 kJ/kg.

Fig. 2. RF configuration with PCM (layer thickness expressed in mm) and sensors position.

3. Monitoring system

The monitoring system included heat flux meters [58] and temperature sensors (T-type thermocouples) [59]. Heat flux meters were made of a thermopile protected by a ceramic plastic composite body, suitable and reliable for long term installations with IP67 protection. T-type thermocouples (copper and constantan) with FEP sheath were selected as the application required a small temperature detector. The distribution of all the sensors in the plan is reported in Fig. 1, which highlights the monitoring of the three different zones, i.e., the red northern one, the red and blue central one and the blue southern one. The positioning of the sensors in section is illustrated in Fig. 2, showing a representative portion of the RF (consistent with both the red northern zone and the blue southern one) where names of the sensors do not include the distinction between the zones.

The monitoring system consisted of:

- two thermocouples above the mortar (T_{conc} in Fig. 2), one under a S27 ThinICE located in the north area of the floor (T_{conc} _27A in Fig. 1) and another one under a S21 ThinICE placed in the south zone (T_{conc} _21D in Fig. 1);
- two thermocouples on two different PCM containers (T_{ti} in Fig. 2), one on a northern S27 ThinICE (T_{ti} _27A in Fig. 1) and one on a southern S21 ThinICE (T_{ti} _21D in Fig. 1);
- two thermocouples under the floor finishing (T_{floor} in Fig. 2), one nearby a northern S27 ThinICE (T_{floor} _27A in Fig. 1) and another one nearby a southern S21 ThinICE (T_{floor} _21D in Fig. 1);
- two heat flux meters (HF in Fig. 2) on two different S27 ThinICE, one plate on a PCM container laying in the north (HF_27A in Fig. 1) and another plate on a PCM container positioned in the central portion of the floor (HF_27B in Fig. 1) (Fig. 3);
- two heat flux meters (HF in Fig. 2) on two different S21 ThinICE, one meter on a container laying in the central area (HF_21C in Fig. 1) and another meter on a PCM container placed in the south zone of the floor (HF_21D in Fig. 1).

An additional thermocouple was installed in the room to monitor indoor air temperature. Technical data of the heat flux meters and of the thermocouples are reported in Table 3.

A weather station [60] equipped with a pyranometer was installed outside the building to acquire air temperature, humidity, wind speed and direction. All the sensors were directly connected to the analogic channels of a datalogger, a DataTaker DT85 series 4 and its channel expansion (CEM20) [61,62]. Furthermore, all the devices mentioned above were configured in the same schedule, data were acquired with a time step of 1 min and stored via FTP in a storage unit.

4. Monitoring results

Analysis of the measurement data for the heating period showed that overheating conditions occurred during sunny and relative warm days due to the poor thermal inertia of the envelope. Without an appropriate control of the system, solar heat gains, together with the contribution of PCM which slowly reduced its heat flux during the transition process, resulted in an excessive increase in indoor air temperature, negatively impacting on thermal comfort and, above all, wasting the PCM energy saving potential. An example of the thermal behaviour of the system is illustrated in Fig. 4, where values of outdoor air temperature (T_{ext}), solar radiation (*Solar rad.*), concrete surface temperature (T_{conc}) under ThinICE and temperature difference between indoor air temperature and the heating setpoint (ΔT) are reported.

Three days (from January 16th to 18th 2021) were considered; the first and the third ones were characterised by the so-called bell-shaped curve corresponding to solar irradiation under no cloud conditions. The chart shows that during these days, despite the RF system turned off towards 9 a.m. (represented by the moment in which T_{conc} started to significantly drop), indoor air temperature continued to increase up to exceed the setpoint temperature by almost 2 °C (grey arrows). Differently, overheating did not occur during the second day, which was characterised by cloudy conditions.

5. Methods

The observed behaviour of the RF has not to be considered negatively. The phenomenon described, due to the thermal inertia of the PCM integrated system, can be exploited and improved by means of automation control according to weather forecasts and potentially following the real time cost of electricity. Indeed, the RF enhanced by the embedded PCM can trust on thermal inertia for around 12–18 h, depending on outdoor air temperature and solar radiation, which directly affect the building thermal load and consequently the latent heat thermal energy storage made available by the PCM. On the other hand, the air-conditioning terminal units could indirectly control and limit the heat exchange with the conditioned air of the room, as the RF system can exchange a limited quantity of heat flux due to its surface thermal resistance.

The main objective of the study is the investigation of the behaviour of the RF system both in heating and in cooling mode under a suitable control strategy and the evaluation of the achievable energy savings and of the consequences on indoor air temperature control by means of TRNSYS, a TRaNsient SYStem simulation program [63,64]. The mathematical model of the RF system had been previously calibrated with the experimental data gathered during the monitoring campaign (started in August 2020) through the monitoring system described above [65]. The same mathematical model and its characteristics were used to implement the RF control routine and run the simulations.

Taking into consideration the thermal behaviour of the PCM integrated RF revealed by the monitoring results, a control loop for the RF system was implemented in the energy analysis of the case study. According to the routine, the room setpoint temperature was reduced (in winter) or increased (in summer) by an offset of 0.5 °C or 1.0 °C as a function of weather forecast. More in detail, two climatic parameters were considered to control the magnitude of the offset, outdoor air temperature and horizontal solar radiation. The last parameter was selected as an indicator of cloudy or clear sky conditions, which is usually considered in weather forecasting. When both parameters

Table 3
Technical data of the monitoring system sensors.

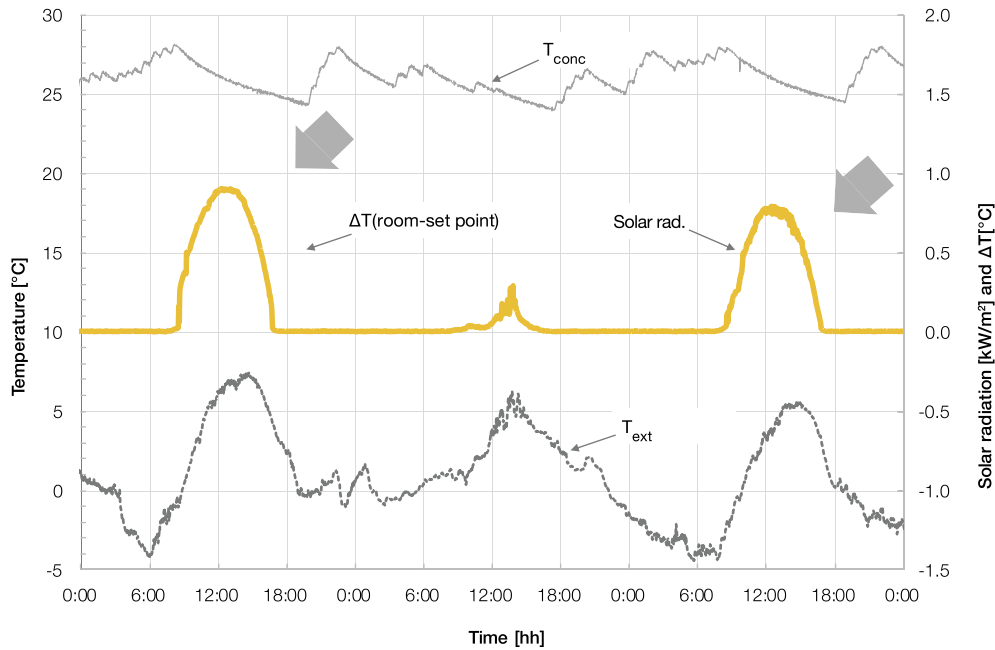|	Sensing area [m^2]	Sensor thickness [m]	Measurement range [W/m^2]	Sensitivity (nominal) [V/(W/m^2)]	Rated operating temperature range [°C]	Uncertainty of calibration
Heat flow meters [58]	8×10^{-4}	5.4×10^{-3}	−2000…+2000	60×10^{-6}	−30 … + 70	± 3 % (k = 2)
	Variant with thermal material	**Accuracy [°C]**	**Measurement range [°C]**			
T-type thermocouples [59]	Cu-CuNi (T)	0.5	−200 to +350			

Fig. 4. Thermal behaviour in winter (Jan, 16th–18th).

exceeded their limit value, the maximum offset was applied to the room setpoint temperature (1 °C). Otherwise, when only one parameter was satisfied, the minimum offset was used (0.5 °C). For the sake of clarity, it is necessary to underline that the small temperature difference selected for the setpoint temperature regulation is not representative of a real case application. Indeed, it is strongly difficult to control indoor air temperature with such a high precision. Rather, the aim of the simulations was to evaluate the tendency of the results obtained if the proposed control strategy would be adopted and compared to a standard approach. This type of control was selected as it is simple to implement in standard plants that are equipped with a minimum of building automation. Indeed, weather forecasts could be shared by national institutions in standard format, or they could be read from a web page and used as source data for the building control system. In the present study, where the control algorithm was implemented in a mathematical model and evaluated through simulations rather than in a real case study, weather forecasts were obtained from the numerical analysis of real monitored weather data used in the simulations as reference weather conditions. In particular, the real weather data of Ferrara for the year 2020 were used, which were collected by the weather station [60] installed outside the demo building. Weather forecast data for outdoor air temperature and horizontal solar radiation were calculated by the energy model in TRNSYS. Each day was divided according to two different time frames, i.e. into sets of 12 h and of 6 h starting from the midnight of every day. Mean values of outdoor air temperature and horizontal solar radiation for each 12-h time frame (or 6-h time frame) were evaluated. Therefore, the obtained average values were constant during each simulation timestep of each 12-h time frame (or 6-h time frame) until the simulation would have considered the next 12-h time frame (or 6-h time frame). This approach is similar to the one adopted by weather forecast services or in weather forecasts commonly available on the web. In Fig. 5 the chart shows how the mean outdoor air temperature is evaluated for the case of 12 h-forecast. As it can be seen in the chart, the mean temperature of the next 12 h is already known by the model of the energy system, and it can be used by the RF control strategy to modify the room setpoint temperature.

6. Energy simulations

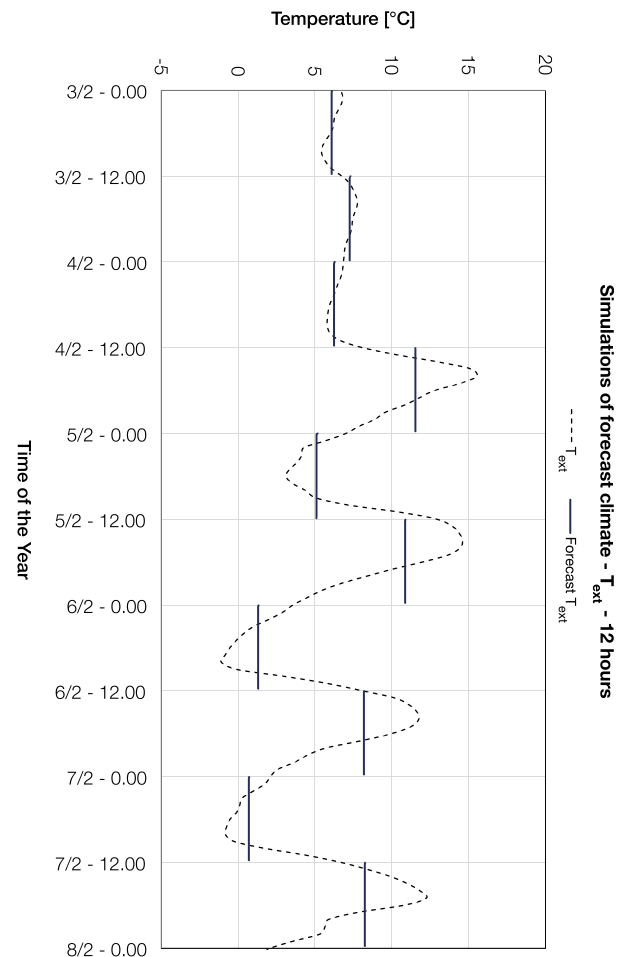The dynamic energy model of the system, including the building and

Fig. 5. Example of weather forecast simulation for a 12-h period.

the RF structure described in the previous section, were developed in TRNSYS environment. The geometric model of the building was generated with Google SketchUp plug-in. The internal volume was divided into three thermal zones, corresponding to the main central test room, equipped with the RF system, and the two guard rooms (Fig. 1). Geometric and thermal properties of the building envelope, air change rate, internal load (sensible and latent), except for the floor, were described in TRNBuild package. The thermal behaviour of the RF integrated with PCM was simulated with the non-standard Type 399 [66] connected to the Type 56 that simulates the building, both in Simulation Studio environment. Type 399 included all the data regarding the RF system (thermophysical properties of the layers, piping pitch and depth, etc.) and was informed by detailed external files – one for the melting and one for the solidification process – created considering the thermal properties of the two different selected PCMs (Table 2) and containing data of specific heat capacity of the PCM in relation to temperature. As only one external file per transition was allowed by Type 399, whilst two different PCMs were adopted in the RF, an equivalent PCM having a mass-averaged specific heat was used to build the external files. The equivalent PCM had then to be scaled to match the actual mass of PCM used in the RF (2.49 kg × n.38 S27 ThinICE and 2.47 kg × n.37 S21 ThinICE). Thermal properties of the building and main boundary conditions used in the simulations are summarised in Table 4.

The first part of the study was aimed at analysing the thermal behaviour of the RF in order to evaluate the energy demand of the system. A set of simulations were carried out for a wide range of couple of values of outdoor air temperature and horizontal solar radiation, the two parameters used as limits for the change of the room setpoint temperature in the proposed control strategy. The routine implemented in the simulations was compared with a reference case study, named RCS, where setpoint temperature was assumed constant and equal to 21 °C and 24 °C throughout the heating and the cooling season respectively. Differently from the RCS, in the weather forecast-based control strategy model, named FCS, the heating and the cooling setpoint temperatures were reduced and increased up to 20 °C and 25 °C respectively according to the values of the average outdoor air temperature and horizontal solar radiation calculated within the 6-h and 12-h time frame. The total heat fluxes exchanged by the heat carrier fluid flowing in the RF piping were calculated for the heating and cooling period over the year of simulation. The couple of parameters which led to the minimum energy demand was used in the following step of the work as limit values for the novel floor control strategy. Values of mean outdoor air temperature and horizontal solar radiation thus assumed for the control strategy were equal to 6 °C with 200 W/m² and 22 °C with 500 W/m² for the heating and cooling period respectively. Therefore, the functionality of the proposed FCS is the following. In the winter season, if weather forecasts for the next 12 h or the next 6 h predict a mean outdoor air temperature higher than 6 °C or a horizontal solar radiation higher than 200 W/m² then the room setpoint temperature,

equal to 21 °C, will be reduced by 0.5 °C. If both the two parameters exceed the limit values the setpoint temperature will be reduced by 1 °C. Considering the cooling period, if the next 12-h or 6-h weather forecasts foreseen a mean outdoor air temperature lower than 22 °C or a horizontal solar radiation lower than 500 W/m² then the room setpoint temperature, equal to 24 °C, will be increased by 0.5 °C. If both the two parameters are lower than the limit values, the setpoint temperature will be increased by 1 °C.

The trend of indoor room temperature was not considered in this first analysis. The heating Q_H and cooling Q_C energy demand of the RF system were calculated on the base of Eq. (1) and Eq. (2) respectively as described in the following:

$$Q_H = \sum \dot{m}_{RF,H} \cdot c \cdot (T_{inRF,H} - T_{outRF,H}) \cdot \Delta t_{step} \tag{1}$$

$$Q_C = - \sum \dot{m}_{RF,C} \cdot c \cdot (T_{inRF,C} - T_{outRF,C}) \cdot \Delta t_{step} \tag{2}$$

where

Q_H, Q_C – total heat exchanged by the RF loop [kJ];
$\dot{m}_{RF,H}, \dot{m}_{RF,C}$ – mass flow rate [kg/h];
c - heat capacity of the fluid [kJ/(kg·°C)];
$T_{inRF,H}, T_{supRF,C}$ – inlet water temperature [°C];
$T_{outRF,H}, T_{retRF,C}$ – outlet water temperature [°C];
Δt_{step} - timestep of the simulation [h].

The calculation has been carried out for the two seasons with a simulation timestep of 5 min. The heating season was considered from 15th October until 15th April according to the national regulation for the city of Ferrara. Out of this period indoor air temperature was controlled by the RF system if it was greater than the cooling setpoint temperature. For the cooling season, differently from the heating one indicated by the national regulation, the period from the beginning of June to mid-September was assumed.

7. Results and discussion

Two sets of simulations were carried out, one considered weather forecasts with a prediction horizon of 12 h (12FCS) and the other one took into account weather forecasts of the following 6-h time frame (06FCS). Results showing the energy savings achievable both on the heating energy demand (Q_H) and on the cooling energy demand (Q_C) by implementing the novel control strategy are summarised in Table 5. In the same table also the main differences in indoor air temperature control are outlined. It could be useful to remind that assumed room setpoint temperatures were equal to 21 °C for the heating and to 24 °C for the cooling season. Overheating and overcooling conditions were identified when the difference between indoor air temperature and the

Table 4
Properties of the building envelope and boundary conditions used in simulations.

Component	Surface [m²]	Thickness [m]	Thermal transmittance [W/(m²·K)]
Wall	39.84	0.12	0.28
Floor	19.08	0.32	0.28
Roof	19.08	0.06	2.08
Boundary conditions		**Value**	**Unit**
Infiltrations		0.10	1/h
Internal loads		110	W
Supply water temperature (heating)		35	°C
Supply water temperature (cooling)		15	°C

Table 5
Main simulation results.

		RCS	12FCS	06FCS
Winter (from 15/10 to 15/04)				
Q_H	[kWh]	1166	1129	1118
Δ Q_H RCS	[%]	–	− 3.2	− 4.2
Troom > 22/<20	[h/h]	1542/274	1309/387	1248/483
Tmin/Tmax	[°C/°C]	18.9/26.0	18.8/25.8	18.9/25.4
Tmean	[°C]	21.7	21.4	21.4
Summer (from 01/06 to 15/09)				
Q_C	[kWh]	546	499	509
Δ Q_C RCS	[%]	–	− 8.6	− 6.7
Troom > 25/<23	[h/h]	567/980	680/821	640/851
Tmin/Tmax	[°C/°C]	20.0/27.2	20.2/27.4	20.2/27.3
Tmean	[°C]	23.6	23.9	23.8

setpoint temperature was higher than 2 °C. For the sake of completeness, a quantitative evaluation of the electric energy savings achieved through the reduction of the operation time of the RF circulator both during the heating and the cooling period are reported in Table 6. In order to aid a proper interpretation of the results it is necessary to underline that the room has a conditioned floor area of about 10 m^2.

As it can be seen in Table 5 a standard control (RCS) generally leads to higher (in winter) and to lower (in summer) values of indoor air temperature (*Tmean* in Table 5), equal to 21.7 °C and to 23.6 °C respectively, compared to the defined setpoint temperatures. Conversely, the average indoor air temperature is always closer to the defined setpoint both in winter and summer by adopting the FCS. Indeed, the hours in which the room temperature exceeds the heating setpoint by more than 1 °C decrease by about 15% with 12FCS and by nearly 19% with 6FCS if compared to RCS. Considering the cooling period, results reported in Table 5 outline that the hours in which indoor temperature falls behind the cooling setpoint by more than 1 °C decrease by almost 16% with 12FCS and by 13% with 6FCS when compared to RCS. At the same time, the hours in which the room temperature is lower or is higher by more than 1 °C than the heating or the cooling setpoint temperature increase when the FCS is adopted. Nevertheless, the maximum (in winter), the minimum (in summer), and the average indoor temperatures obtained with the control loop are closer to the defined setpoint temperature than those achieved in the RCS.

A comparative analysis of the thermal behaviour of the system for the two control strategies is reported in Figs. 6-13. The charts show the trend of the room indoor air temperature during the heating and the cooling period.

Performance of the system with the 12FCS case study for a week in early March and during a week in mid-December are illustrated in Figs. 6 and 8. The same analysis is reported for the 06FCS in Figs. 7 and 9. The chart in Fig. 6 illustrates the positive effect achieved on indoor temperature in winter – early March – by adopting the 12FCS, especially during the second and the third day of the week. More in detail, the reduction in the setpoint temperature (*12FCS - T$_{set\_H}$*) – implemented on the basis of the favourable weather forecasts of the following 12 h – avoids the unnecessary turning on of the RF (*12FCS – ON-OFF*) and reduces peak in indoor temperature by more than 0.5 °C (*12FCS - T$_{room}$*). Indeed, the quite high outdoor temperature or the high horizontal solar radiation foreseen in the following 12 h result in lower transmission heat losses or solar heat gains which, together with the thermal inertia provided by the PCM, do not require the turning on of the RF. The switching on of the RF system is postponed to the morning of the third day. Weather forecast data thus allow to exploit and maximise the energy benefits of the PCM. Differently, in the last days of the week both room temperature and operating period of the RF system present slight differences between the two control strategies (Figs. 6 and 7).

Taking into consideration the second winter week selected, in mid-December (Fig. 8), similar observations can be reported for the trends of indoor temperature with and without the 12FCS. Nevertheless, whilst the setpoint temperature is extremely variable over the week in early March (Fig. 6), during this week it is constant and equal to 20.5 °C (Fig. 8). This means that one of the two parameters considered – outdoor air temperature and horizontal solar radiation – always exceeded the
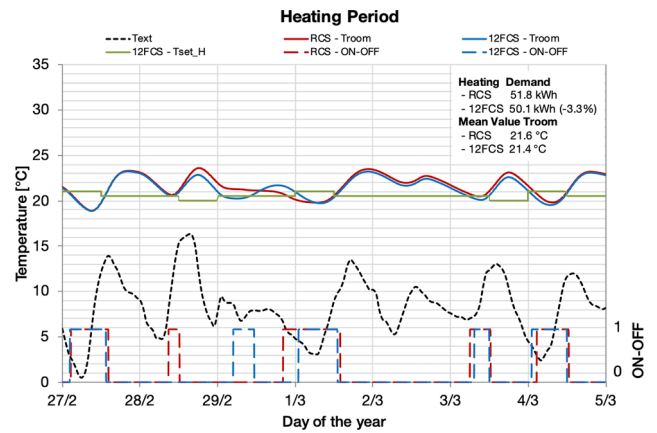

Fig. 6. Comparison of RCS and 12FCS – Heating period from 27/02 to 04/03.
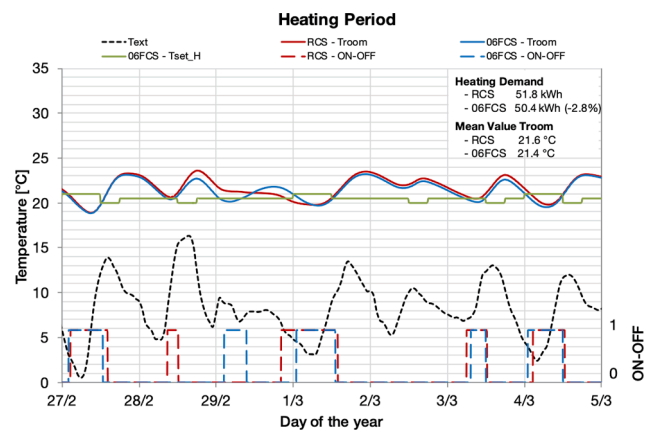

Fig. 7. Comparison of RCS and 06FCS – Heating period from 27/02 to 04/03.

limit value defined to make the setpoint temperature be reduced by 0.5 °C. The chart shows good results in terms of indoor air temperature control when the control loop is adopted. More in detail, the routine avoids overheating for a long time during the second day. Room temperature is on average lower than the defined setpoint for the remaining days of the week, but it is still within an acceptable range. As regards the operating time of the RF system, it works for a shorter period than in the RCS. This leads to energy savings on the electric absorption of the circulator of the RF loop, summarised in Table 6. The same observations can be reported for the 06FCS illustrated in Fig. 9.

Taking into account the cooling season, the thermal behaviour of the system under the 12FCS during a week in mid-July and for a week in early August is reported in Figs. 10 and 12, while results for the 06FCS case study considering the same periods are illustrated in Figs. 11 and 13.

Results for the 12FCS (Figs. 10 and 12) show that improvement in indoor temperature control is less evident if compared to the results

Table 6
Energy savings on the electric energy demand of the RF circulator.

	RCS		12FCS			06FCS		
	Operating time [h]	Q_{EL} [kWh]	Operating time [h]	Q_{EL} [kWh]	Δ Q_{EL} RCS [%]	Operating time [h]	Q_{EL} [kWh]	Δ Q_{EL} RCS [%]
Winter (W)*	1224	30.6	1164	29.1	−4.9	1137	28.4	−7.1
Summer (S)**	1211	36.3	1018	30.5	−15.9	1070	32.1	−11.6
W + S	2435	66.9	2182	59.6	−10.9	2207	60.5	−9.6

*Constant speed of the circulator, power absorption 25 W.
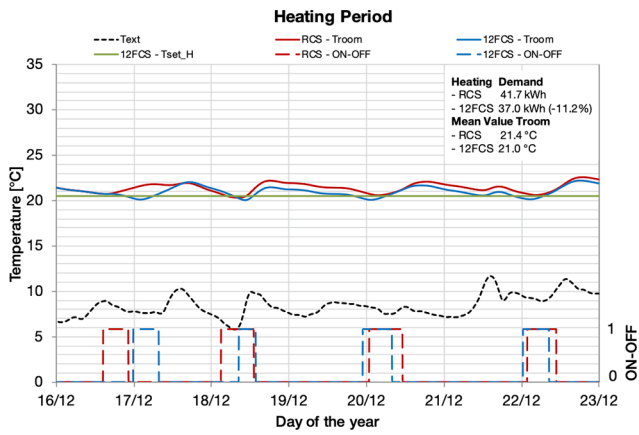**Constant speed of the circulator, power absorption 30 W.

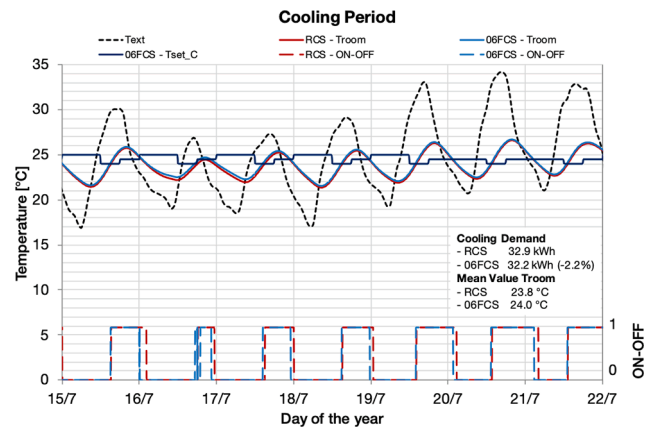**Fig. 8.** Comparison of RCS and 12FCS – Heating period from 16/12 to 22/12.

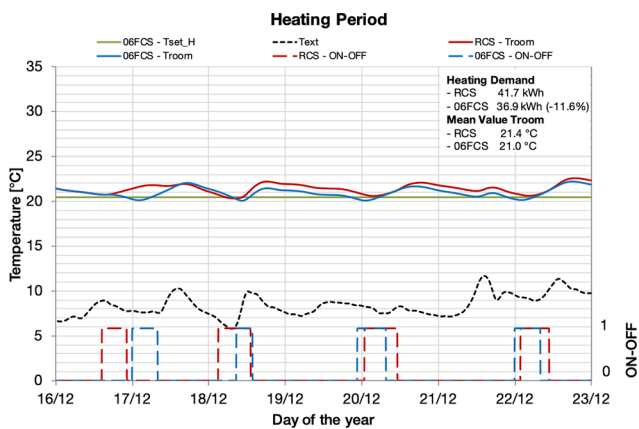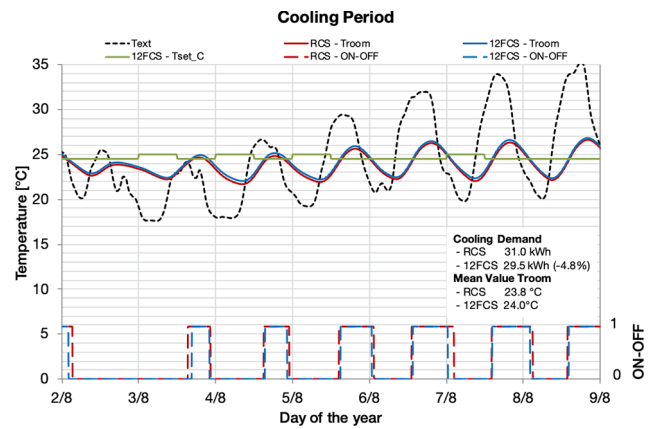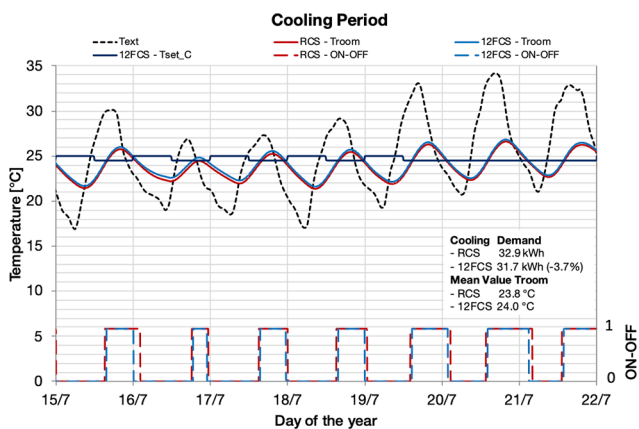**Fig. 9.** Comparison of RCS and 06FCS – Heating period from 16/12 to 22/12.

Fig. 10. Comparison of RCS and 12FCS – Cooling period from 15/07 to 21/07.

Fig. 11. Comparison of RCS and 06FCS – Cooling period from 15/07 to 21/07.

Fig. 12. Comparison of RCS and 12FCS – Cooling period from 02/08 to 08/08.
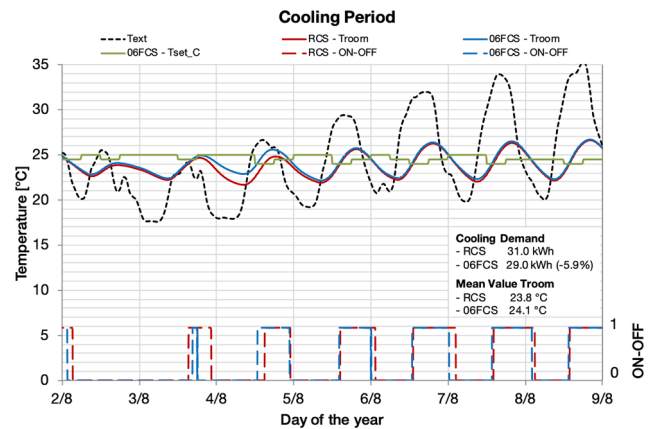

Fig. 13. Comparison of RCS and 06FCS – Cooling period from 02/08 to 08/08.

obtained for the heating (Figs. 6 and 8). Reduction in temperature peak is very small. Nevertheless, average value of room temperature is always closer to the setpoint with the adoption of the control loop. Furthermore, operation time of the RF system is lower than in the RCS. Achievable energy savings on cooling energy demand during these weeks were estimated to range between 4% and about 5% compared to the RCS. Considering the 06FCS (Figs. 11 and 13), a significant difference from the 12FCS emerges for the week in early August (Fig. 13). For this period indoor temperature is higher with 06FCS than with 12FCS between August 4th and 5th. Indeed, during the second day the RF system is

switched on for less time with 06FCS, thus avoiding the overcooling of the room. Differently, the other days were characterised by the room overcooling with both the control loops, i.e., 12FCS and 06FCS.

Whilst Figs. 6, 8, 10 and 12 illustrate results for the floor control strategy with a prediction horizon of 12 h (12FCS), charts in Figs. 7, 9, 11 and 13 consider the floor control strategy with a prediction horizon of 6 h (06FCS). In this case, as the setpoint temperature is controlled with a 6-h time frame, the curve representing it is decisively more variable over the time than with a 12-h control. However, a preliminary comparative analysis between results achieved for 12FCS and for 06FCS does not

uncover significant differences, except for the week in early August mentioned before (Figs. 12 and 13).

Simulation results demonstrated that the implementation of the control strategy for the RF system allows to obtain energy savings both on heating and on cooling energy demand due to a peak shaving of the maximum and minimum indoor air temperature of the room. In particular, cuts in heating energy demand ranged from 3% to 11% for both the control strategies, while energy savings on cooling energy demand ranged from about 4% to 5% for 12FCS, and from about 2% to 6% for 06FCS. However, if average energy savings for the whole heating period were considered (Table 5), these were equal to about 3% and to nearly 4% for the 12FCS and for the 06FCS respectively. Average energy savings on cooling energy demand were equal to almost 9% and 7% for the 12FCS and for the 06FCS respectively. As regards the electric energy savings achievable through the reduction of the operation time of the RF circulator, data reported in Table 6 highlight that about 10% could be reached both with the 12FCS and the 06FCS. Similarly to what was observed for the energy savings achievable on the heating and on the cooling energy demand, the adoption of the 12FCS resulted to be more effective during the cooling season while the 06FCS brought to higher energy savings during the heating period.

Fig. 14 illustrates the heat flux exchanged by the RF with the test room during the heating period. The liquid mass fraction of the equivalent PCM (S21 and S27) integrated in the RF system is also reported, which highlights the melting and solidification process of the PCM linked to the RF operation. The fluctuation of the heat flux is obviously affected by the PCM, indoor air temperature and the switching on of the RF system. When the RF is operating the PCM begins the melting phase and its liquid mass fraction increases. During this process the PCM stores latent heat that is made available again and slowly released by the PCM when the RF system is turned off. Against this background, when favourable weather conditions are foreseen for the following 12 or 6 h, the RF is turned off in advance in order to exploit the latent heat thermal energy storage of the PCM and maximise its energy saving potential.

8. Conclusions and outlook

The monitoring campaign revealed some issues related to the management of the PCM integrated RF coupled with the lightweight envelope of the test-building. More in detail, data for the heating season highlighted overheating conditions in correspondence of sunny and relative warm days. A suitable control strategy based on weather forecasts was developed with the aim of investigating the thermal behaviour of the RF system and the related energy saving potential. The following outputs were obtained from the present study:

- Weather forecast data can be used to mitigate overheating and overcooling issues.
- Outdoor air temperature and sky conditions (clear or cloudy) forecasting can be used as parameters for the management of the control strategy of the RF.
- The simple routine used in the simulations estimated energy savings equal to about 4% and 8% on the heating and on the cooling energy demand respectively.
- The adoption of weather forecasts with a prediction horizon of 12 h is better for the heating period, while a prediction horizon of 6 h is better for the cooling period. This tendency is verified also when energy savings on the electric energy demand of the RF circulator are considered.

One of the future developments of the study will be the application of the proposed control strategy to the large-scale prototype of the PCM integrated RF that will be installed in the large demo-building of IDEAS project to be realised in Ferrara by the end of 2021. In this application a RF structure different from the one illustrated in Fig. 2 will be installed. The new PCM enhanced RF will have piping adjacent on the above surface of PCM containers.
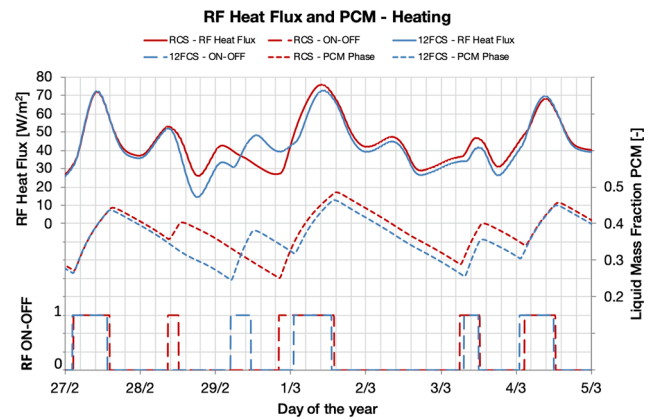

Fig. 14. Example of RF behaviour in the heating season.

Declaration of Competing Interest

The authors declare that they have no known competing financial interests or personal relationships that could have appeared to influence the work reported in this paper.

Acknowledgements

References

[1] I. Adilkhanova, S.A. Memon, J. Kim, A. Sheriyev, A novel approach to investigate the thermal comfort of the lightweight relocatable building integrated with PCM in different climates of Kazakhstan during summertime, Energy 217 (2021), 119390, https://doi.org/10.1016/j.energy.2020.119390.

[2] O. Flodén, Vibrations in Lightweight Structures - Efficiency and Reduction of Numerical Models, Lund University, 2014.

[3] A. Jeanjean, R. Olives, X. Py, Selection criteria of thermal mass materials for low-energy building construction applied to conventional and alternative materials, Energy Build. 63 (2013) 36–48, https://doi.org/10.1016/j.enbuild.2013.03.047.

[4] K. Gregory, B. Moghtaderi, H. Sugo, A. Page, Effect of thermal mass on the thermal performance of various Australian residential constructions systems, Energy Build. 40 (4) (2008) 459–465, https://doi.org/10.1016/j.enbuild.2007.04.001.

[5] A. Sharma, V.V. Tyagi, C.R. Chen, D. Buddhi, Review on thermal energy storage with phase change materials and applications, Renew. Sustain. Energy Rev. 13 (2) (2009) 318–345, https://doi.org/10.1016/j.rser.2007.10.005.

[6] L.F. Cabeza, I. Martorell, L. Miro, A. Fernández, C. Barreneche, Introduction to thermal energy storage systems, in: L.F. Cabeza (Ed.), Advances in Thermal Energy Storage Systems, Second Edition, Woodhead Publishing, Elsevier, Cambridge, 2021, pp. 1–33, https://doi.org/10.1016/B978-0-12-819885-8.00001-2.

[7] R.A. Kishore, M.V.A. Bianchi, C. Booten, J. Vidal, R. Jackson, Modulating thermal load through lightweight residential building walls using thermal energy storage and controlled precooling strategy, Appl. Therm. Eng. 180 (2020), 115870, https://doi.org/10.1016/j.applthermaleng.2020.115870.

[8] T. Li, A. Merabtine, M. Lachi, N. Martaj, R. Bennacer, Experimental study on the thermal comfort in the room equipped with a radiant floor heating system exposed to direct solar radiation, Energy 230 (2021), 120800, https://doi.org/10.1016/j.energy.2021.120800.

[9] Y. Xia, X.S. Zhang, Experimental research on a double-layer radiant floor system with phase change material under heating mode, Appl. Therm. Eng. 96 (2016) 600–606, https://doi.org/10.1016/j.applthermaleng.2015.11.133.

[10] R. Ansuini, R. Larghetti, A. Giretti, M. Lemma, Radiant floors integrated with PCM for indoor temperature control, Energy Build. 43 (11) (2011) 3019–3026, https://doi.org/10.1016/j.enbuild.2011.07.018.

[11] B. Larwa, S. Cesari, M. Bottarelli, Study on thermal performance of a PCM enhanced hydronic radiant floor heating system, Energy 225 (2021), 120245, https://doi.org/10.1016/j.energy.2021.120245.

[12] R. Barzin, J.J.J. Chen, B.R. Young, M.M. Farid, Application of PCM underfloor heating in combination with PCM wallboards for space heating using price based control system, Appl. Energy 148 (2015) 39–48, https://doi.org/10.1016/j.apenergy.2015.03.027.

[13] W. Cheng, B. Xie, R. Zhang, Z. Xu, Y. Xia, Effect of thermal conductivities of shape stabilized PCM on underfloor heating system, Appl. Energy 144 (2015) 10–18, https://doi.org/10.1016/j.apenergy.2015.01.055.

[14] S. Lu, Y. Zhao, K. Fang, Y. Li, P. Sun, Establishment and experimental verification of TRNSYS model for PCM floor coupled with solar water heating system, Energy Build. 140 (2017) 245–260, https://doi.org/10.1016/j.enbuild.2017.02.018.

[15] M. Zhao, T. Zhu, C. Wang, H. Chen, Y. Zhang, Numerical simulation on the thermal performance of hydraulic floor heating system with phase change materials, Appl. Therm. Eng. 93 (2016) 900–907, https://doi.org/10.1016/j.applthermaleng.2015.10.020.

[16] W. Fu, T. Zou, X. Liang, S. Wang, X. Gao, Z. Zhang, Y. Fang, Thermal properties and thermal conductivity enhancement of composite phase change material using sodium acetate trihydrate-urea/expanded graphite for radiant floor heating system, Appl. Therm. Eng. 138 (2018) 618–626, https://doi.org/10.1016/j.applthermaleng.2018.04.102.

[17] Y. Fang, Y. Ding, Y. Tang, X. Liang, C. Jin, S. Wang, X. Gao, Z. Zhang, Thermal properties enhancement and application of a novel sodium acetate trihydrate-formamide/expanded graphite shape-stabilized composite phase change material for electric radiant floor heating, Appl. Therm. Eng. 150 (2019) 1177–1185, https://doi.org/10.1016/j.applthermaleng.2019.01.069.

[18] L. Royon, L. Karim, A. Bontemps, Thermal energy storage and release of a new component with PCM for integration in floors for thermal management of buildings, Energy Build. 63 (2013) 29–35, https://doi.org/10.1016/j.enbuild.2013.03.042.

[19] X. Jin, X. Zhang, Thermal analysis of a double layer phase change material floor, Appl. Therm. Eng. 31 (10) (2011) 1576–1581, https://doi.org/10.1016/j.applthermaleng.2011.01.023.

[20] Y. Xu, B.B. Sun, L.J. Liu, X.Y. Liu, The numerical simulation of radiant floor cooling and heating system with double phase change energy storage and the thermal performance, J. Energy Storage 40 (2021), 102635, https://doi.org/10.1016/j.est.2021.102635.

[21] W. Sun, Y. Zhang, Z. Ling, X. Fang, Z. Zhang, Experimental investigation on the thermal performance of double-layer PCM radiant floor system containing two types of inorganic composite PCMs, Energy Build. 211 (2020), 109806, https://doi.org/10.1016/j.enbuild.2020.109806.

[22] J. Jeon, J.-H. Lee, J. Seo, S.-G. Jeong, S. Kim, Application of PCM thermal energy storage system to reduce building energy consumption, J. Therm. Anal. Calorim. 111 (1) (2013) 279–288, https://doi.org/10.1007/s10973-012-2291-9.

[23] J. Mazo, M. Delgado, J.M. Marin, B. Zalba, Modeling a radiant floor system with Phase Change Material (PCM) integrated into a building simulation tool: analysis of a case study of a floor heating system coupled to a heat pump, Energy Build. 47 (2012) 458–466, https://doi.org/10.1016/j.enbuild.2011.12.022.

[24] I. Cerón, J. Neila, M. Khayet, Experimental tile with phase change materials (PCM) for building use, Energy Build. 43 (8) (2011) 1869–1874, https://doi.org/10.1016/j.enbuild.2011.03.031.

[25] A.G. Entrop, H.J.H. Brouwers, A.H.M.E. Reinders, Experimental research on the use of micro-encapsulated Phase Change Materials to store solar energy in concrete floors and to save energy in Dutch houses, Sol. Energy 85 (5) (2011) 1007–1020, https://doi.org/10.1016/j.solener.2011.02.017.

[26] A. Ozadowicz, J. Grela. Impact of building automation control systems on energy efficiency - University building case study, in: Proceedings of 22nd IEEE International Conference on Emerging Technologies and Factory Automation (ETFA), 2017. Limassol, Cyprus, September 12–15.

[27] X. Shi, S.A. Memon, W. Tang, H. Cui, F. Xing, Experimental assessment of position of macro encapsulated phase change material in concrete walls on indoor temperatures and humidity levels, Energy Build. 71 (2014) 80–87, https://doi.org/10.1016/j.enbuild.2013.12.001.

[28] A. Mavrigiannaki, E. Ampatzi, Latent heat storage in building elements: a systematic review on properties and contextual performance factors, Renew. Sustain. Energy Rev. 60 (2016) 852–866, https://doi.org/10.1016/j.rser.2016.01.115.

[29] H. Mirinejad, S.H. Sadati, M. Ghasemian, H. Torab, Control techniques in heating, ventilating and air conditioning (HVAC) systems, J. Comput. Sci. 4 (9) (2008) 777–783, https://doi.org/10.3844/jcssp.2008.777.783.

[30] F. Behrooz, N. Mariun, M.H. Marhaban, M.A.M. Radzi, A.R. Ramli, Review of control techniques for HVAC systems-nonlinearity approaches based on fuzzy cognitive maps, Energies 11 (2018) 495, https://doi.org/10.3390/en11030495.

[31] J. Joe, P. Karava, A model predictive control strategy to optimize the performance of radiant floor heating and cooling systems in office buildings, Appl. Energy 245 (2019) 65–77, https://doi.org/10.1016/j.apenergy.2019.03.209.

[32] A. Aswani, N. Master, J. Taneja, A. Krioukov, D. Culler, C. Tomlin, Energy-efficient building HVAC control using hybrid system LBMPC, IFAC Proc. Vol. 45 (17) (2012) 496–501.

[33] A. Afram, F. Janabi-Sharifi, Theory and applications of HVAC control systems - A review of model predictive control (MPC), Build Environ. 72 (2014) 343–355, https://doi.org/10.1016/j.buildenv.2013.11.016.

[34] S. Sakunthala, R. Kiranmayi, P. Nagaraju Mandadi, Soft computing techniques and applications in electrical drives fuzzy logic, and genetic algorithm, Helix 8 (2018) 3285–3289, https://doi.org/10.29042/2018-3285-3289.

[35] A. Saberi Derakhtenjani, A.K. Athienitis, Model predictive control strategies to activate the energy flexibility for zones with hydronic radiant systems, Energies 14 (2021) 1195, https://doi.org/10.3390/en11030495.

[36] F. D'Ettorre, P. Conti, E. Schito, D. Testi, Model predictive control of a hybrid heat pump system and impact of the prediction horizon on cost-saving potential and optimal storage capacity, Appl. Therm. Eng. 148 (2019) 524–535, https://doi.org/10.1016/j.applthermaleng.2018.11.063.

[37] M. Luzi, M. Vaccarini, M. Lemma, A tuning methodology of Model Predictive Control design for energy efficient building thermal control, J. Build. Eng. 21 (2019) 28–36, https://doi.org/10.1016/j.jobe.2018.09.022.

[38] Y. Zong, G.M. Böning, R.M. Santos, S. You, J. Hu, X. Han, Challenges of implementing economic model predictive control strategy for buildings interacting with smart energy systems, Appl. Therm. Eng. 114 (2017) 1476–1486, https://doi.org/10.1016/j.applthermaleng.2016.11.141.

[39] R. Barzin, J.J.J. Chen, B.R. Young, M.M. Farid, Application of weather forecast in conjunction with price-based method for PCM solar passive buildings – An experimental study, Appl. Energy 163 (2016) 9–18, https://doi.org/10.1016/j.apenergy.2015.11.016.

[40] A. Kelman, Y. Ma, F. Borrelli. Analysis of local optima in predictive control for energy efficient buildings, in: Proceedings of the 50th IEEE Conference on Decision and Control and European Control Conference, 2011, pp. 5125–5130. Orlando, FL, USA, December 12–15, 10.1109/ CDC.2011.6161498.

[41] E. Biyik, J.D. Brooks, H. Sehgal, J. Shah, S. Gency, Cloud-based model predictive building thermostatic controls of commercial buildings: algorithm and implementation, in: Proceedings of the 2015 American Control Conference (ACC), 2015, pp. 1683–1688. Chicago, IL, USA, July 1–3, 10.1109/ACC.2015.7170975.

[42] B. Celik, R. Roche, S. Suryanarayanan, D. Bouquain, A. Miraoui, Electric energy management in residential areas through coordination of multiple smart homes, Renew. Sustain. Energy Rev. 80 (2017) 260–275, https://doi.org/10.1016/j.rser.2017.05.118.

[43] K. Shan, S. Wang, C. Yan, F.u. Xiao, Building demand response and control methods for smart grids: a review, Sci. Technol. Built Environ. 22 (6) (2016) 692–704, https://doi.org/10.1080/23744731.2016.1192878.

[44] S. Merabti, B. Draoui, F. Bounaama, A review of control systems for energy and comfort management in buildings, in: Proceedings of the 8th International Conference on Modelling, Identification and Control (ICMIC), 2016, pp. 478–486. Algiers, Algeria, November 15-17, 10.1109/ICMIC.2016.7804161.

[45] M. Kolokotroni, M.D.A.E.S. Perera, D. Azzi, G.S. Virk, An investigation of passive ventilation cooling and control strategies for an educational building, Appl. Therm. Eng. 21 (2) (2001) 183–199, https://doi.org/10.1016/S1359-4311(00)00008-9.

[46] M. Fiorentini, G. Serale, G. Kokogiannakis, A. Capozzoli, P. Cooper, Development and evaluation of a comfort-oriented control strategy for thermal management of mixed-mode ventilated buildings, Energy Build. 202 (2019), 109347, https://doi.org/10.1016/j.enbuild.2019.109347.

[47] G. Gholamibozanjani, M. Farid, A critical review on the control strategies applied to PCM-enhanced buildings, Energies 14 (2021) 1929, https://doi.org/10.3390/en14071929.

[48] P. Devaux, M.M. Farid, Benefits of PCM underfloor heating with PCM wallboards for space heating in winter, Appl. Energy 191 (2017) 593–602, https://doi.org/10.1016/j.apenergy.2017.01.060.

[49] K. Lin, Y. Zhang, H. Di, R. Yang, Study of an electrical heating system with ductless air supply and shape-stabilized PCM for thermal storage, Energy Convers. Manag. 48 (2007) 2016–2024, https://doi.org/10.1016/j.enconman.2007.01.014.

[50] K. Faraj, J. Faraj, F. Hachem, H. Bazzi, M. Khaled, C. Castelain, Analysis of underfloor electrical heating system integrated with coconut oil-PCM plates, Appl. Therm. Eng. 158 (2019), 113778, https://doi.org/10.1016/j.applthermaleng.2019.113778.

[51] G. Serale, M. Fiorentini, A. Capozzoli, P. Cooper, M. Perino, Formulation of a model predictive control algorithm to enhance the performance of a latent heat solar thermal system, Energy Convers. Manag. 173 (2018) 438–449, https://doi.org/10.1016/j.enconman.2018.07.099.

[52] C.R. Touretzky, M. Baldea, A hierarchical scheduling and control strategy for thermal energy storage systems, Energy Build. 110 (2016) 94–107, https://doi.org/10.1016/j.enbuild.2015.09.049.

[53] A.C. Papachristou, C.A. Vallianos, V. Dermardiros, A.K. Athienitis, J.A. Candanedo, A numerical and experimental study of a simple model-based predictive control strategy in a perimeter zone with phase change material, Sci. Technol. Built Environ. 24 (9) (2018) 933–944, https://doi.org/10.1080/23744731.2018.1438011.

[54] IDEAS – Novel building Integration Designs for increased Efficiencies in Advanced Climatically Tunable Renewable Energy Systems. https://www.horizon2020ideas.eu [Accessed 10th September 2021].

[55] ThinICE Phase Change Material. https://www.pcmproducts.net/files/ThinICE.pdf [Accessed 10th September 2021].

[56] PCM Products Ltd. https://www.pcmproducts.net [Accessed 10th September 2021].

[57] PCM Products Ltd, PlusICE Hydrated Salt (S) Range, 2018. https://www.pcmproducts.net/files/S%20range-C2018.pdf [Accessed 10th September 2021].

[58] HFP01 heat flux sensor. https://www.hukseflux.com/products/heat-flux-sensors/heat-flux-meters/hfp01-heat-flux-sensor [Accessed 10th September 2021].

[59] Delta strumenti, thermocouple wire (in Italian). https://www.deltastrumenti.it/images/pdf/termocoppie/in_cavetto/Termocoppia_cavetto.pdf [Accessed 10th September 2021].

[60] Weather station Vantage Pro2. https://www.davisinstruments.com/vantage-pro2/ [Accessed 10th September 2021].

[61] DT85 Series 4 Data Logger. https://assets.thermofisher.com/TFS-Assets/ANZ/brochures/datatoker-dt85-series-4-data-logger.pdf [Accessed 10th September 2021].

[62] CMe3000. https://www.elvaco.se/en/product/infrastructure1/cme3000-m-bus-gateway-for-fixed-network–1050015 [Accessed 10th September 2021].

[63] A. Athienitis, W. O'Brien, Modeling, Design, and Optimization of Net-Zero Energy Buildings, Ernst & Sohn, 2015.

[64] S.A. Klein, W.A. Beckman, J.W. Mitchell, J.A. Duffie, N.A. Duffie, T.L. Freeman, J. C. Mitchell, J.E. Braun, B.L. Evans, J.P. Kummer, et al., TRNSYS Version 18, Solar Energy Laboratory, University of Wisconsin-Madison, 2018.

[65] S. Cesari, A. Natali, B. Larwa, E. Baccega, M. Boschetti, E. Mainardi, M. Cavazzuti, A. Piazzi, G. Mangherini, D. Vincenzi, M. Bottarelli, A heat pump-based multi-source renewable energy system for the building air conditioning: the IDEAS project experience, Ital. J. Eng. Sci. 65 (2021) 12–22, https://doi.org/10.18280/ti-ijes.650102.

[66] D. Arno, S. Wolfram, Trnsys User Manual, Type 399: Phase change materials in passive and active wall constructions, Georg Simon University of Applied Sciences, Institute for Energy and Building, 2020.